JAST, Vol. 14, No 1, pp 128-142
© Iranian Aerospace Society, winter-spring 2021

JAST
Journal of Aerospace Science and Technology

Science Article

Model Predictive Fault Tolerant Control of Two-Tethered Satellite System

Mahya Ramezani[1], Nima Assadian[2*]
1- Faculty of New Sciences and Technologies, University of Tehran
2- Department of Aerospace Engineering, Sharif University of Technology, Tehran
*Postal code;1458889694, Tehran, Iran
Email: ***assadian@sharif.edu**

The purpose of this paper is to propose a method for the dual space tether system to continue its mission in the event of a failure by using fault-tolerant control. To accomplish this, a new and accurate model of a space tether with two tethers has been introduced, which can demonstrate the effects of the tensile force more precisely in the model. One of the features of this model is the ability to modify the junction of the tethers to the subsatellite, which can be included as a control parameter in the problem. As a result, the fuel required to control the mission can be decreased. To mitigate the effects of tether failure, a fault-tolerant control strategy based on model predictive control (MPC) has been developed for the nonlinear space tether system. This control method has the advantage of being both optimal and capable of controlling the system in the event of a failure. The simulation results demonstrate that the proposed control method is capable of controlling the dual spatial tether system despite thruster and tether failure.

Keywords: *Space tether system, fault-tolerant control, nonlinear model predictive control, attitude and position control.*

Nomenclature

$\boldsymbol{a}$	Difference equations vector of state variables
A	Cross-section of tether
$\mathbf{C}_I^i$	Transfer matrix from inertial system to ith-satellite
$\boldsymbol{e_r}$	The unit vector in the direction of the orbital radius of the satellite
E	Modulus of elasticity of the tether
$\boldsymbol{F}$	Force vector
$\boldsymbol{H}$	Satellite angular momentum vector
$\mathbf{I}$	Satellite moment of inertia matrix
J	Cost function (criterion function) of the model predictive control
$\boldsymbol{L}$	Tether length
m	Satellite mass
$\boldsymbol{M}$	Total moments applied to the satellite
N	Horizon length
$\boldsymbol{P}$	Tether junction
$\boldsymbol{q}$	Quaternion vector
$\mathbf{Q}$	The weight matrix of the cost function related to the reference trajectory tracking
$\boldsymbol{r}$	Satellite orbital radius
R_{spool}	Pulley radius
$\mathbf{R}$	The weight matrix of the cost function related to the control effort
$\boldsymbol{T}$	The tension force of the tether
$\boldsymbol{u}$	Vector of control inputs
w	Angle velocity of pulley
$\boldsymbol{x}$	State variables vector
μ	Earth gravitational parameter
$\boldsymbol{\omega}$	The angular velocity vector of the satellite body
$\boldsymbol{\Omega}$	The skew-symmetric matrix of the angular velocity vector of Quaternion equations

1 PhD student
2 Professor, Corresponding Author

Received: 31 May 2021
Accepted: 24 July 2021

$\mathbb{1}$	Step function of the tether tension (for negative tension, the value is zero)

Subscripts

0	Related to free conditions of the tether
A, B	Related to the satellites A and B
g	Related to the gravity
i, j	Related to the i^{th} and j^{th} satellite or tether
r	Reference trajectory index
RW	Related to the reaction wheel
T	Related to the tether tension
Th	Related to the thrust
x, y, z	Vector elements in x, y, and z directions of the body axes

Superscripts

i	The vector in the i^{th} satellite body system
I	The vector in the inertial system
T	Transpose

Introduction

Space tethers are long cables made of strong fibers or conductive wires that connect two or more satellites. The motion of the space tether system can be analyzed in three phases: deployment, steady-state, and retraction. Although space exploration did not begin until the mid-20th century, the concept of using a tether as a space elevator was first proposed in 1895 [1]. Numerous missions have been accomplished via space tethers, including the Charge-1 in 1983, Charge-2 in 1985, Oedipus-A in 1989, Oedipus-C in 1995, TSS-1 in 1992, TSS-1R in 1996, SESD-1 in 1993, SESD-2 in 1994, PMG (Plasma Motor generator) in 1993 [2], TIPS in 1996 [3], YES in 1997 [4], YES2 in 2007 [5], Atex in 1998 [6], and Mast in 2007 [7].

Tethers are frequently used in space missions for a variety of purposes, including artificial gravity on the space station, cargo transfer missions between orbits, injecting satellites into the desired orbit, performing orbital maneuvers with minimum fuel consumption, and studying the outer layers of the atmosphere. One of the most critical applications of space tethers is the use of robots to collect space debris [8]. Space debris disposal has become a fundamental requirement in recent decades as a result of the increase in space debris. As a result, a new class of satellites has been introduced as space tether robots. Due to the requirement to collect space debris, it is critical to reach the desired position and orientation of the space tether, particularly the subsatellite.

One of the disadvantages of using the space tether system is the high probability of the tether being torn, resulting in the mission's failure. A solution to this problem is to use high-performance systems for the tether's deployment and retraction phases or to use multiple tethers rather than a single tether. However, the risk of mission failure in space tethers has always been a major concern. The purpose of this research is to introduce fault-tolerant control based on model predictive control to continue the space tether system's mission in the event of a failure by stabilizing the motion of satellites.

Another difficulty with advanced systems is their precise control, which is complicated by the system's coupled nonlinear dynamics. Significant research has been conducted in this field over the last few decades. Misra and Diamond have developed a space tether system that connects two satellites via two tethers that are both massless and expandable. The results indicate that using two tethers rather than one improves the rotational behavior of the system [9]. Kumar [10] adjusted the length of the tether using a hybrid control method to control the tether satellite system connected to the two tethers. The distance between the junction of the tethers and the center of mass imposes additional torque on the model, which results in the coupling between translational and rotational motion of the tethered system [11]. Three models implementing distinct control strategies (tether junction, thruster-based control, and stress-based control, as well as their combination) have been compared. The results indicate that the optimal system for rejecting disturbances is the combination of these strategies [12]. Moreover, the simultaneous position control of two satellites connected via tether has been investigated using the sliding mode control method in [13]. Other researchers have investigated the feasibility of using the tether junction on the primary satellite to eliminate the vibrations generated along the tether. However, it was demonstrated that when the tether's structure is considered flexible and elastic, the system becomes unstable [14]. To avoid missions failing following a failure, Godard utilized offset control to implement adaptive fault-tolerant control in the presence of a tether failure [15-16].

Two satellites orbiting in a circular orbit are mostly considered to be two-point masses

connected by one or more rigid tethers with uniform mass distribution [17-18]. Due to the mathematical simplicity of the model, it has been widely used to simulate dynamics and to evaluate various control methods during various phases of satellite operation. However, due to the complexity of the real environment, more accurate models are required. For instance, in the studies conducted with the system in the elliptical orbit, modifications were made to the turbulence of the tether control, increasing the complexity of the control [19-20]. Additionally, in modeling the space debris removal tethered satellites systems of most previous studies, the position of the satellites is assumed to be independent of the satellite's attitude and the attitude and position of the tethers, which is not a valid assumption [21].

Due to the complexity of the model, conventional control methods cannot be used to control the dynamics of space tethered satellite systems. Additionally, as previously stated, another issue associated with the tether system is tether failure. To cope with the effects of tether failure, fault-tolerant control methods should be used. Feng used fault-tolerant control to monitor the attitude of an over-actuated satellite in the presence of actuator loss or fault and external disturbances [22]. Jin et al. proposed a straightforward and effective fault-tolerant control strategy for a four-wheel reaction satellite [23].

Optimal methods are among the control methods that are good at controlling nonlinear models. Model predictive control (MPC) is an advanced method of optimal control. This method utilizes the model to predict the output of the system over a finite time horizon and to calculate the optimal input [24]. Another feature of this method is the trade-off with various constraints, which is frequently used due to the constraints associated with tether systems, particularly those that utilize reaction wheels. MPC is widely used in space applications due to the aforementioned characteristics. MPC techniques have been applied to a variety of applications, including monitoring the attitude of satellites [25] and controlling space robots and tether systems [26]. An MPC method is used for a satellite in case of losing a thruster [27]. Similarly, in [28] employing the MPC method, the coupled rotational and translational dynamics of a satellite is controlled in the event of a thruster failure. In another research, the MPC is used for the formation flight of satellites and it was demonstrated that by utilizing real-world constraints, the desired control can be accomplished through the use of MPC [29].

The purpose of this study is to control the deployment and retraction phases of the space tether system. Two tethers connect the main satellite to the sub-satellite, and the attachment points on the main satellite and sub-satellite are initially symmetrically oriented away from the center of mass. The attitude and position of the main and sub-satellites are inextricably linked to the tethers' internal and external movements. The longitudinal vibration of the tethers is calculated due to their elasticity. The system is controlled via the reaction wheel, thruster, and tension control of the tethers. One of the tethers is assumed to fail in different phases of the mission. Naturally, it should be noted that tether failure is diagnosed using a different system, and this issue is not addressed in this study.

The second section of this paper presents the dynamic model of the tether before and after failure. The third section introduces fault-tolerant control based on model predictive control. The fourth section presents the simulation results for the proposed system and control for various mission phases and also investigates the control system's capability under various conditions and in the presence of uncertainties using Monte-Carlo simulation. Finally, the concluding remarks are presented.

Dynamic Analysis of Tether Satellite System Connected to Two Tethers

The governing equations of the system are derived in this section, including the dynamic equations of attitude and position of satellites and tethers.

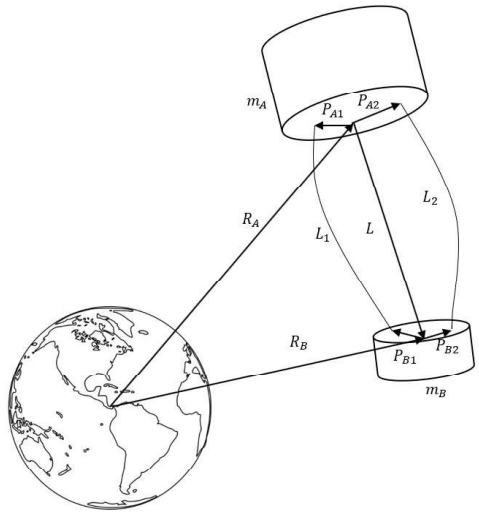

Fig. 1. Schematic of a satellite system with two tethers.

As illustrated in Fig 1, the system is composed of a primary satellite with a mass of m_A and a subsatellite with a mass of m_B, which are initially connected by two flexible massless tethers, but one of the tethers tears after a while. Notably, deformation of the tether is not considered when it is in compression. The system orbits in an elliptical orbit around the Earth. Three reaction wheels and three thrusters control both the main satellite and the subsatellite. It should be noted that the junction of the tethers (P_{B1} and P_{B2}) to the subsatellite is assumed to be adjustable and has been used as a control parameter. The purpose of this mechanism is to adjust the length of the tether tension arm to maximize tether traction and generate the desired torque for controlling the subsatellite's attitude. It is worth noting that a comprehensive examination of this mechanism is beyond the scope of this article; what is required is that the tether's junction with the satellite's surface can be controlled via the satellite's control arms. Each tether's length is determined by a pulley on the primary satellite, the equations for which are provided. The tethers were deployed and retracted using a combination of pulleys and thrusters connected to the subsatellite. Aerodynamic forces have been considered negligible. It is assumed that the tether will not collide with the other tether and satellites after it is cut. Tether motion in three-dimensional space is studied. The disturbances caused by a tether rupture have been ignored. The fault detection system works autonomously, and fault data is fed into the system autonomously.

Governing Equations

For the primary satellite A, a body system is defined; its center is located at the center of mass of the satellite, and its axis directions are aligned with the primary axes of satellite A. This system is called A. We mount a body system dedicated to the subsatellite; its center is aligned with the center of mass of the satellite B, and its axes align with the axes of the primary satellite B. This system is called B. The inertial coordinate system is centered on the earth center, with its z-axis aligned with the earth's rotational axis, its x-axis aligned with the direction of the equinox, and its y-axis completing the right-handed coordinate system.

Rotational Dynamic Equations of the Satellites

The governing equations are introduced in the inertial system first, and then in the body system [30]. It is worth noting that $\boldsymbol{X}^{y}$ represents the $\boldsymbol{X}$ vector elements are expressed in the y coordinate system. Euler's equations of angular motion in the body axes of both satellites are:

$$\frac{d\boldsymbol{H}_i^i}{dt} + \boldsymbol{\omega_i} \times \boldsymbol{H}_i^i = \boldsymbol{M}_i \qquad i = A, B \qquad (1)$$

$\boldsymbol{M}_i$ denotes the total external torques applied to the i^{th} satellite, which include gravitational gradient torques, tether torques, and reaction wheel torques. $\boldsymbol{H}_i^i$ refers to the angular momentum vector of the satellite, and $\boldsymbol{\omega}_i = [\boldsymbol{\omega}_{x_i} \quad \boldsymbol{\omega}_{y_i} \quad \boldsymbol{\omega}_{z_i}]^T$ is the angular velocity vector of the i^{th}-satellite body. The direction and magnitude of the tether traction forces, $\boldsymbol{T}_i$ are required to determine the $\boldsymbol{M}_{T_{i|j}}$ torque, which is the torque applied by the j^{th}-tether to the i^{th}-satellite. The length vector of the tethers in the inertial system is as follows:

$$\boldsymbol{L}_j^I = \boldsymbol{L}^I + \boldsymbol{P}_{B_j}^I - \boldsymbol{P}_{A_j}^I \qquad j = 1,2 \qquad (2)$$

Where

$$\boldsymbol{T}_j^I = \frac{\boldsymbol{L}_j^I + \boldsymbol{P}_{B_j}^I - \boldsymbol{P}_{A_j}^I}{|\boldsymbol{L}_j|} \qquad j = 1,2 \qquad (3)$$

$\boldsymbol{L}_j^I$ refers to the j^{th}-tether vector in inertia, $\boldsymbol{P}_{i_j}^I$ is the junction of the j^{th}-tether to i^{th}-satellite, and L^I is the vector of the distance between two satellite mass centers in the inertial frame.

Hooke's law states that the force exerted by the tethers in the inertial frame is as follows:

$$\boldsymbol{F}_{T_{A|j}}^I = -\boldsymbol{F}_{T_{B|j}}^I = \boldsymbol{T}_j^I A_j E_j \left(\frac{L_j - L_{j_0}}{L_{j_0}}\right).\mathbb{1}_j$$
$$j = 1,2 \qquad (4)$$

Where A_j is the cross-section, E_j is the elastic modulus of the tether, and L_{j_0} is the free-state length of the j^{th} tether. $\mathbb{1}_j$ is the step function that, when the tether's tension is negative, sets the force of the tether to zero. The rotation matrix is used to express this force in the body coordinate systems. The following equation can be used to calculate the gravity gradient torque [32]:

$$\boldsymbol{M}_{g_i} = \frac{-3\mu}{|r_i|^3}\,\mathbf{C}_l^i\,\boldsymbol{e}_{r_i} \times \left(\mathbf{I}_i\,\mathbf{C}_l^i\,\boldsymbol{e}_{r_i}\right) \quad i = A, B \tag{5}$$

Where $\boldsymbol{M}_{g_i}$ is the torque due to gravity gradient applied to the i^{th}-satellite, $\boldsymbol{r}_i$ is the i^{th}-satellite orbital radius, and $\mathbf{C}_l^i$ is the transfer matrix from inertial coordinate system to the i^{th}-satellite body coordinate system. $\boldsymbol{e}_{r_i}$ is the unit vector for i^{th}-satellite orbital radius. The equation governing the satellites' attitude is obtained by transferring to its body systems and decoupling the angular momentum of the satellite body and the reaction wheel. The satellite's Euler equations are as follows:

$$\mathbf{I}_i\dot{\boldsymbol{\omega}}_i^i = \boldsymbol{M}_{g_i}^i + \sum_{j=1}^{2}\boldsymbol{M}_{T_{i|j}}^i + \boldsymbol{M}_{RW_i} - \boldsymbol{\omega}_i \times \left(\mathbf{I}_i\boldsymbol{\omega}_i^i + \mathbf{I}_{RW_i}\boldsymbol{\omega}_{RW_i}\right) - \mathbf{I}_{RW_i}\dot{\boldsymbol{\omega}}_{RW_i} \quad i = A, B \tag{6}$$

Where $\boldsymbol{M}_{T_{i|j}}$ is the torque due to the tension of the j^{th}-tether on the i^{th}-satellite, and $\boldsymbol{M}_{\mathrm{RW}_i}$ is torque from the i^{th}-satellite reaction wheels. $\mathbf{I}_i$ and $\mathbf{I}_{RW_i}$ are the moments of inertia matrices of the i^{th}-satellite and reaction wheels, respectively. $\boldsymbol{\omega}_{RW_i}$ is the angular velocity vector of the i^{th}-satellite reaction wheel. Due to the singularity in Euler's angles differential equations, the attitude of each satellite is represented using quaternions with the following differential equations [33]:

$$\dot{\boldsymbol{q}}_i = \frac{1}{2}\boldsymbol{\Omega}_i\boldsymbol{q}_i \quad i = A, B \tag{7}$$

In which

$$\boldsymbol{\Omega}_i = \begin{bmatrix} 0 & \boldsymbol{\omega}_{z_i} & -\boldsymbol{\omega}_{y_i} & \boldsymbol{\omega}_{x_i} \\ -\boldsymbol{\omega}_{z_i} & 0 & \boldsymbol{\omega}_{x_i} & \boldsymbol{\omega}_{y_i} \\ \boldsymbol{\omega}_{y_i} & -\boldsymbol{\omega}_{x_i} & 0 & \boldsymbol{\omega}_{z_i} \\ -\boldsymbol{\omega}_{x_i} & -\boldsymbol{\omega}_{y_i} & -\boldsymbol{\omega}_{z_i} & 0 \end{bmatrix} \tag{8}$$

It is worth noting that the torque applied to the satellites by the tethers can be calculated by determining their tension and their junction points with respect to the bodies of the satellite.

Transitional Equations

Newtonian approach is used to derive the satellite transitional equations of motion [34].

The equations are obtained in the inertial coordinate system as follows:

$$m_i\ddot{\boldsymbol{r}}_i^I = \boldsymbol{F}_{g_i}^I + \sum_{j=1}^{2}\boldsymbol{F}_{T_{i|j}}^I + \boldsymbol{F}_{Th_i}^I \quad i = A, B \tag{9}$$

$$\boldsymbol{R}_B = \boldsymbol{R}_A + \boldsymbol{L} \tag{10}$$

Where $\ddot{\boldsymbol{r}}_i^I$ is the acceleration to the center of the mass of the satellites A and B, m_i is the mass of the i^{th}-satellite, $\boldsymbol{F}_{g_i}^I$ is the gravitational force vector applied to the i^{th}-satellite, $\boldsymbol{F}_{T_{i|j}}^I$ is the tensile force vectors of the j^{th}-tether, and $\boldsymbol{F}_{Th_i}^I$ is the control vector of the propulsion system of the i^{th}-satellite.

Based on Newton's law of gravity, $\boldsymbol{F}_{g_i}^I$ is equal to

$$\boldsymbol{F}_{g_i}^I = \frac{\mu m_i}{|\boldsymbol{r}_i^I|^3}\boldsymbol{r}_i^I \tag{11}$$

The length of the tethers is assumed to be controlled by pulleys embedded in the primary satellite:

$$\dot{L}_{j_0} = R_{spool}w_j \qquad j = 1,2 \tag{12}$$

Where R_{spool} is the radius and w_j is the angular velocity of the j^{th}-satellite pulley, respectively, which w_j is considered as a control input. The instantaneous length of each arc can be calculated using the satellites' attitude and position.

Satellite Model After Rupture of a Tether

One of the tethers is assumed to have been ruptured due to vibrations in the system. In this case, it is sufficient to consider one of the tensions as zero; the equations are as follows:

$$\frac{d\boldsymbol{H}_i^i}{dt} + \boldsymbol{\omega}_i \times \boldsymbol{H}_i^i = \boldsymbol{M}_{g_i}^i + \boldsymbol{M}_{T_{i1}}^i + \boldsymbol{M}_{RW_i} \tag{13}$$

$$m_i\ddot{\boldsymbol{r}}_i^I = \boldsymbol{F}_{g_i}^I + \boldsymbol{F}_{T_{i|1}}^I + \boldsymbol{F}_{Th_i}^I \quad i = A, B \tag{14}$$

Fault-Tolerant Control Based on Model Predictive Control

Fault-Tolerant Control

This control method is designed in such a way that, in the event of a fault, it can avoid the mission failing and handle the faults by making a series of appropriate decisions. Generally, fault-tolerant control methods employ a variety of scenarios. The primary criteria for classifying these methods and applying them to the required scenarios are

mathematical design tools, design methods, a configuration mechanism or model, and operators and systems that must be traded off to avoid fault [35].

Model predictive control is a frequently used technique in fault-tolerant control. Model predictive control can easily decide to control the system in the event of a failure due to the predictive nature of controller design, the ability to manage control variable constraints, and the state and capability of this method in handling nonlinear systems. Due to the fact that this controller is designed in such a way that control is assigned based on the system model, in the event of a system failure, the control effort required to control the system is calculated and applied to the system based on the available actuators. However, it is evident that better results would be obtained if the dynamic model is modified following the failure to predict future system output based on the failure.

Model Predictive Control

Model predictive control (MPC) is a sophisticated technique for monitoring and controlling multivariable systems. If there is an appropriate model of the system, this control method can be used. Using an optimizer and predicting the output of the system over a finite time horizon, this control method determines the optimal control decision at any time and applies it to the system. Generally, the primary goal of optimization is to minimize a cost function. The predictive model's control calculations are designed to identify a sequence of control variables that would optimize the predictive model's response to reference points. The block diagram in Fig. 2 depicts the MPC method.

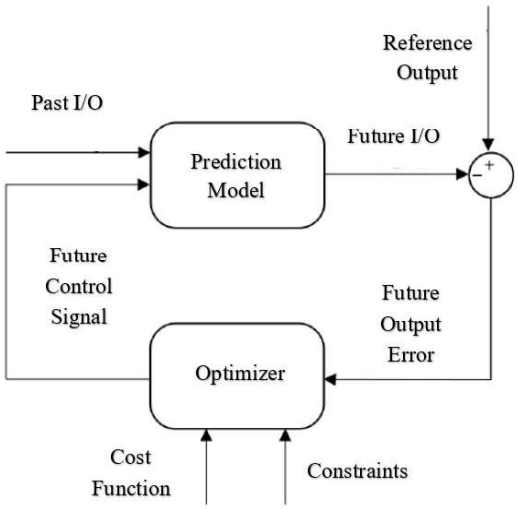

Fig. 2. Block diagram of the model predictive controller

In a tracking problem, the control system has to determine inputs in such a way that the system state variables are close to the reference trajectory. This means that if we wish to keep the state variables on the reference variable, the control system must be designed in such a way that it is capable of maintaining the system in the desired state. The central concept of model predictive control, which applies to both linear and nonlinear systems, is to predict and optimize future behavior using the model. One of the advantages of this control method is that control is allocated stage by stage. This is accomplished by allocating control effort among actuators based on the weight of the control variables, which makes it simple to determine the appropriate value of each input. The cost function, which must be optimized at each time step based on the system performance predictions over a finite time horizon, and thus the control signal to be applied to the dynamic system at the current time, are defined as follows:

$$J = \sum_{i=0}^{N-1}\big(\boldsymbol{x}(i) - \boldsymbol{x}_r(i)\big)^T \mathbf{Q}\big(\boldsymbol{x}(i) - \boldsymbol{x}_r(i)\big) + \big(\boldsymbol{u}^T(i)\mathbf{R}\boldsymbol{u}(i)\big) \quad (15)$$

Where $\boldsymbol{x}(i)$ is the state variables, $\boldsymbol{x}_r(i)$ reference trajectory, and $\boldsymbol{u}(i)$ is the i^{th} control input vector. N is the prediction horizon, and $\mathbf{Q}$ and $\mathbf{R}$ are the weighting positive-definite matrices.

It should be noted that the vector defining the control input is as follows:

$$\boldsymbol{u} = \left[\boldsymbol{F}_{Th_A}^{A} \quad \boldsymbol{F}_{Th_B}^{B} \quad w_1 \quad w_2 \quad \boldsymbol{\omega}_{RW_A} \quad \boldsymbol{\omega}_{RW_B} \quad P_{B_1} \quad P_{B_2}\right] \tag{16}$$

The objective of the model predictive controller is to minimize the proposed cost function as expressed in the difference equation below:

$$\boldsymbol{x}(k+1) = \boldsymbol{a}(\boldsymbol{x}(k), \boldsymbol{u}(k), \boldsymbol{k}) \tag{17}$$

Where k refers to the time step.

Additionally, the model predictive control method allows for the modeling of the system's constraints. In this regard, the cost function is optimized at any point in time to satisfy the system's constraints, ensuring that the system is always operating within its constraints. The system is constrained by the upper limit of the thruster, the maximum rotational rate of the pulleys, which determines the maximum rate of change of the tether's length, and the tether's connection to the subsatellite. After a certain point, reaction wheels can no longer increase their angular velocity, which is referred to as the reaction wheel saturation phenomenon. As a result, saturation prevention constraints should be considered for the system to ensure that the wheel's angular velocity does not exceed a specified value.

Numerical Simulation

The following section presents numerical simulations of fault-tolerant control performance using model predictive control. The deployment and retraction phases of the tether satellite system have been considered for this purpose. The system parameters and characteristics are presented in Table 1.

Table 1. The system characteristics of the space tether [15].

Parameter	Value	Parameter	Value
m_A (kg)	40	$\boldsymbol{P}_{A1}$	$[0.25 \quad 0.25 \quad -0.125]^T$
m_B (kg)	8.3	$\boldsymbol{P}_{A2}$	$[-0.25 \quad -0.25 \quad -0.125]^T$
$\mathbf{I}_A$ (N.m^2)	diag([0.324 0.303 0.486])	$\boldsymbol{P}_{B1}$	$[0.2 \quad 0.2 \quad 0.15]^T$
$\mathbf{I}_B$ (N.m^2)	diag([0.137 0.178 0.176])	$\boldsymbol{P}_{B2}$	$[-0.2 \quad -0.2 \quad 0.15]^T$
A_1 (m^2)	10^{-6}	A_2 (m^2)	10^{-6}
R_{spool} (m)	0.06	$\boldsymbol{r}_A$ (m)	$[0 \quad 6.5 \quad 1]^T \times 10^6$
E (N/m)	2.4×10^{11}	$\dot{\boldsymbol{r}}_A$ (m/s)	$[7 \quad 0 \quad 0]^T \times 10^3$

Each satellite in this system is equipped with orthogonal thrusters mounted on the principal body axes of the satellite. These thrusters do not generate torque in the satellite and are solely used to generate control forces for position control. Additionally, each satellite has three orthogonal reaction wheels aligned with the satellites' principal body axes. It should be noted that the numerical simulation was performed using the fourth-order Runge-Kutta method and the interior point method as the optimizer. The system is first simulated without control to demonstrate the system's instability, and then with the introduced control method, the space tether system is controlled in both failure and non-failure conditions during the deployment and retraction phases. Five steps were considered prior to the failure, and ten steps were considered following the failure.

The proposed control method is used in this section to control the space tether system both with and without failure. To accomplish this, the system was first controlled without failure and with all actuators and then investigated in the event of one of the tethers failing and the propulsion system failing due to a tether rupture.

Tables 2 and 3 detail the control method's settings and the system's constraints, respectively. The fluctuations in the time history graphs are caused by the size of the time steps used to simulate the control method. As a result of the control method's discrete nature, the output is discrete with a fixed step size.

Table 2. Control system parameters.

Parameter	Value	Parameter	Value
dt (s)	0.2	N	10
$\mathbf{Q}$	$\mathrm{diag}([1_{9\times1} \quad 10_{9\times1}])$	$\mathbf{R}$	$\mathrm{diag}([1_{16\times1}])$

Table 3. System constraints.

Parameter	Range	Parameter	Range
$\boldsymbol{F}_{Th_A}$ (N)	$[-1 \quad 1]$	$\boldsymbol{\omega}_{spool}$ (rpm)	10
$\boldsymbol{F}_{Th_B}$ (N)	$[-0.5 \quad 0.5]$	$P_{B1} = P_{B2}$ (m)	0.3

Deployment of the Space Tether System without Failure

The space tether system is considered without failure during this phase. Table 4 summarizes the initial and final conditions (boundary conditions) considered in this scenario.

Table 4. Initial and desired conditions of the space tether system without failure.

Variable	Initial Condition	Desired Condition
$\boldsymbol{L}$ (m)	$[3 \quad 4 \quad 5]^T$	$[8 \quad 9 \quad 10]^T$
$\dot{\boldsymbol{L}}$ (m/s)	$[0 \quad 0 \quad 0]^T$	$[0 \quad 0 \quad 0]^T$
($\phi \quad \theta \quad \psi$)	[90 0 90]	[90 0 90]
$\boldsymbol{\omega}_{A,B}$ (Deg/s)	$[0 \quad 0 \quad 0]^T$	$[0 \quad 0 \quad 0]^T$

As is well known, the satellites' attitude should be maintained throughout the mission while their distance is increased. It is also assumed that the tethers' connections to the body is fixed and uncontrollable in this simulation scenario. Fig. 3 illustrates the evolution of the satellites' relative positions during the system deployment phase with two tethers in the presence of the control method. According to the graph, the system's command was executed perfectly appropriately, and the system was able to perform the desired deployment. Although the convergence speed has slowed at the end of the trajectory due to the optimization of the fuel consumption parameter, it is clear that the system will converge with increasing time.

The time-domain behavior of the satellites' angles and angular velocities when the proposed control method is used is shown in Figures 4 and 5, respectively. As illustrated in these graphs, the control system was successful in maintaining the satellites' attitude within the desired range. The slight changes in the satellite's attitude are caused by the tensile force of the tether, which imparts undesirable torque on the system but which the system has been able to eliminate.

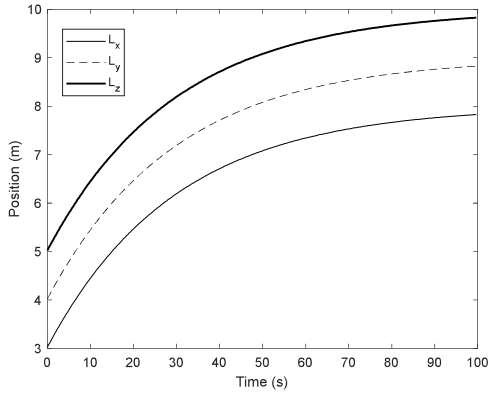

Fig. 3. Distance between two satellites in the tether deployment phase without failure.

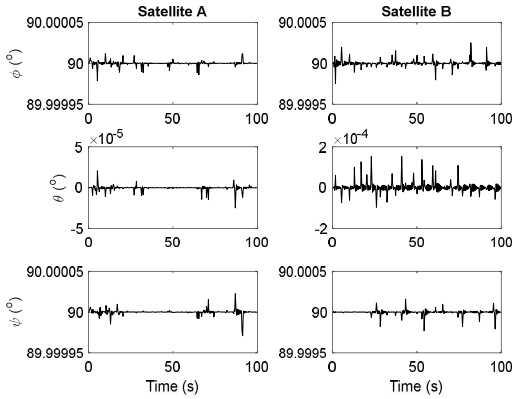

Fig. 4. Attitude of the angles of the satellites in the presence of control in the tether deployment phase without failure.

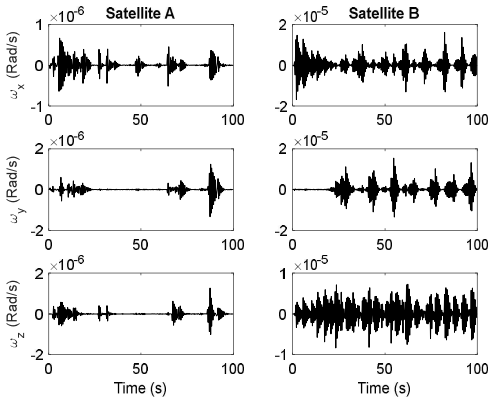

Fig. 5. Angular velocities of the satellites in the presence of control in the tether deployment phase without failure.

The variations in the forces exerted by the thrusters on the satellites are shown in Fig. 6 and demonstrate that the value of thrust remains within the allowable range and the constraints are satisfied (according to Table 3). The reaction wheels' angular velocities are shown in Fig. 7 to offset the torque generated by the tethers, which are known to have low values and change slowly, and thus do not require a large change in angular velocity in a short period. Additionally, Fig. 8 depicts the evolution of the tethers' lengths over time. It is obvious that changes in the length of the tethers are gradual and do not occur abruptly, implying that they do not lose control.

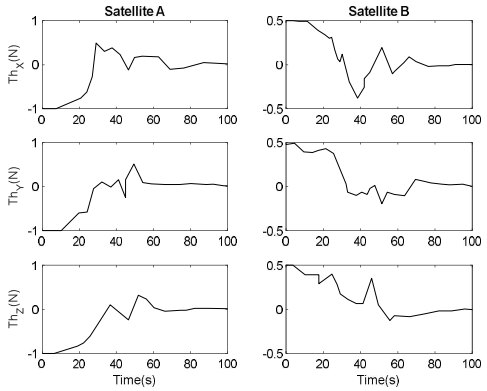

Fig. 6. The control efforts applied by the thrusters in the deployment phase of the tether without failure.

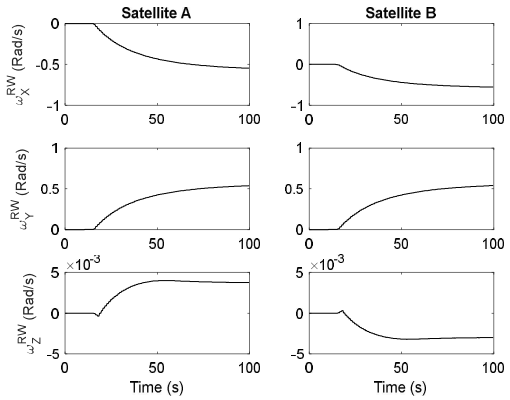

Fig. 7. The control efforts applied by the reaction wheel to the system in the deployment phase without failure.

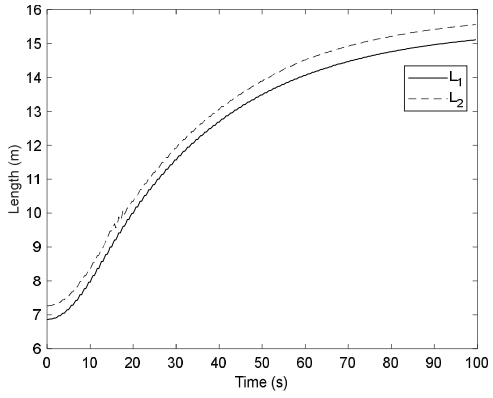

Fig. 8. Graph of increasing the length of the tethers by pulleys in the deployment phase of the tether without failure.

Retraction Phase in the Presence of Satellite A Thrusters and Tether Failures

Space tether retraction is considered in this scenario, assuming the satellite A thruster is failed. Additionally, it is assumed that due to the tether failure, satellite A was in rotation, and this should be eliminated. As a worst-case scenario, it is assumed that satellite A either lacks a thruster or has a damaged thruster. It should be noted that thruster and tether failures are distinct, and to determine the ability of the control method to control the faulty system, one of the satellites' thrusters is also assumed to be failing (in the worst-case scenario). As with the previous scenario, it is assumed that the junction of the tether remains unchanged.

The distance between the two satellites is shown in Fig. 9 following the application of the control command. As can be seen, the system successfully executed the control command, which resulted in the placement of the two satellites at the specified locations and the retraction phase is done completely. The tether length graph of Fig. 10 is plotted as a function of time during the retraction phase following a tether loss. It is obvious that the tether's length has decreased as the distance between the satellites decreases, allowing it to use traction to reduce the amount of thrust required to change the distance. However, this torque resulted in undesirable torque in the system. It should be noted that the pulley does not control the tether force; rather, the pulley controls the tether length.

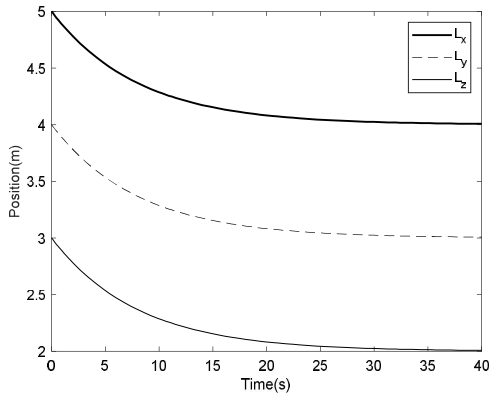

Fig. 9. The distance between two satellites during the retraction phase in the presence of failures of the satellite A thruster and a tether.

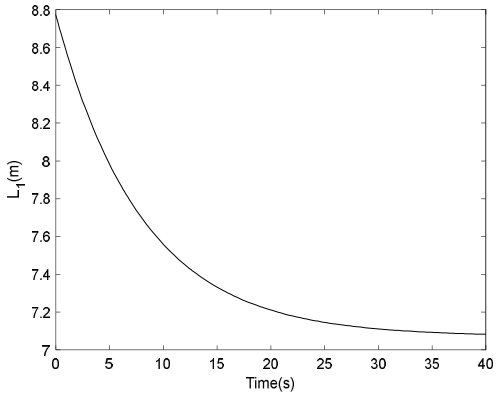

Fig. 10. The tether length during the retraction phase in the presence of failures of the satellite A thruster and a tether.

Figs. 11 and 12 illustrate the satellites' Euler angles and angular velocities. Clearly, the attitude of satellite A has been controlled and converged to the desired value. However, because the tether is retracting, the tether applied unintentional torque to the satellite B, causing periodic disturbances, but the control method was able to repel these disturbances effectively. Fig. 13 illustrates the reaction wheels' angular velocities, which can track the desired reference by generating the torque required to eliminate perturbations. Fig 14 shows the control efforts exerted by the satellite's thrusters, with the satellite A thrusters turned off and only the satellite B thrusters capable of applying force. As the distance between the two satellites increases, the thrusters apply more force, and as the desired value approaches, the amount of force required decreases.

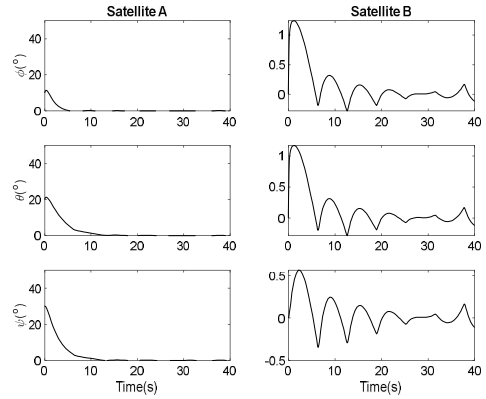

Fig. 11. The Euler angles of the satellites in the retraction phase in the presence of the failures of satellite A thrusters and a tether.

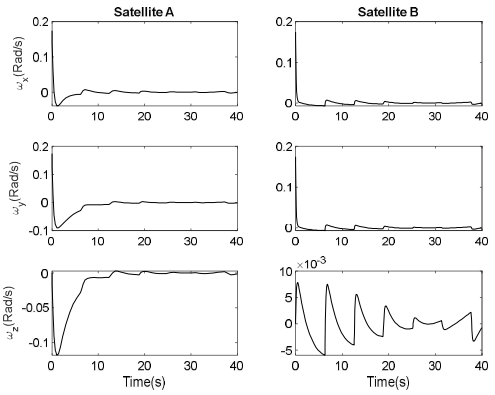

Fig. 12. The angular velocities of the satellites in the retraction phase in the presence of the failures of satellite A thrusters and a tether.

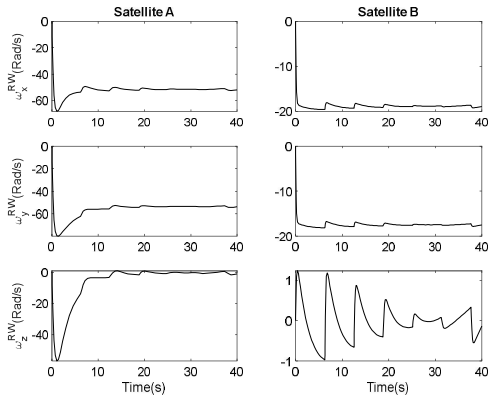

Fig. 13. The angular velocities of the reaction wheels in the retraction phase in the presence of failures of the satellite A thrusters and a tether.

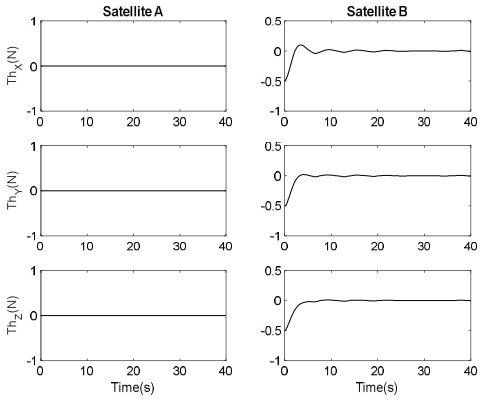

Fig. 14. The control efforts of the thrusters in the retraction phase in the presence of failures of the satellite A thrusters and a tether.

Simulation of Deployment Phase for the Case of the Tether Failure

We have simulated the deployment phase in this section if one of the tethers is lost. The simulations

demonstrate that the system was able to maintain proper control and complete the mission despite the failure. It should be noted that to investigate the effect of changing the control method's parameters on system performance, the value of Q was increased tenfold from the value introduced in the previous scenarios, which should result in the system being controlled more quickly. Fig. 15 illustrates the distance between two tethers following the loss of a tether during the deployment phase. As demonstrated in the simulation, the system is perturbed when attempting to execute the desired command. Later, approximately 4 seconds later, the tether becomes tensile, and through tensile control, the tether accomplishes the required goal. The resulting disturbances are damped in a timely manner, and the system is well equipped to control the resulting conditions. Figs. 16 and 17 illustrate the angular velocity and attitude of satellites, which, as can be seen, are disturbed by the tension of the tether due to the tether's and satellites' position coupled with each another and move away from the specified reference, and reverts to the reference trajectory via the reaction wheels.

Figs. 18 and 19 illustrate the control torque values maintained within the allowable range by the reaction wheels and thrusters, respectively. Fig. 20 illustrates the tether's junction to satellite B, which minimizes tension generated by changing the junction points and thus avoids disturbances caused by the torque on the attitude angles. Additionally, it is observed that the satellites have reached their final state and stabilized in a much shorter period of time than before.

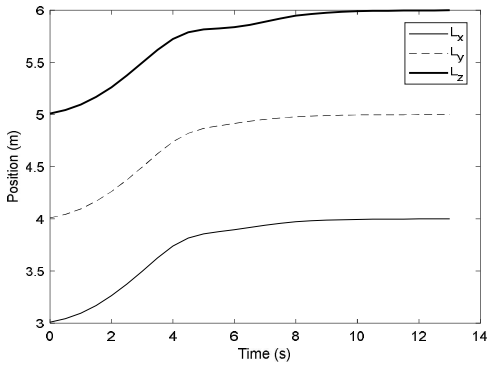

Fig. 15. The distance of two satellites relative to each other in the deployment phase in case of failure of a tether.

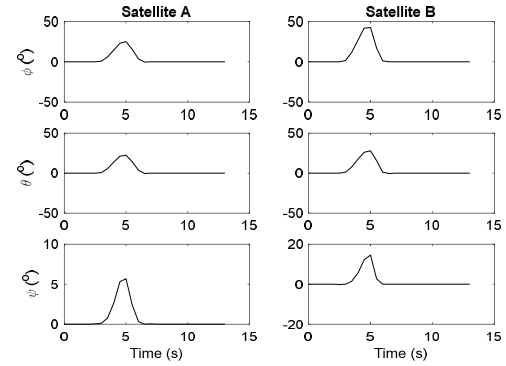

Fig. 16. The position of the angles of the satellites in the deployment phase in case of failure of a tether.

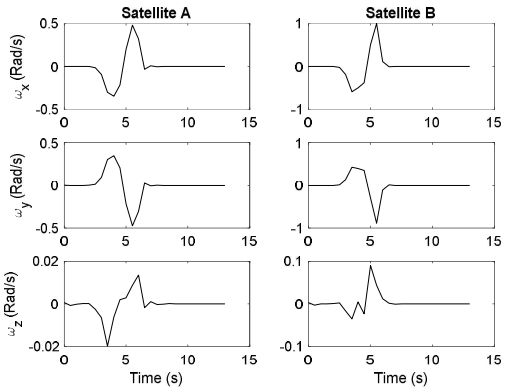

Fig. 17. The angular velocities of the satellites in the deployment phase in case of failure of a tether.

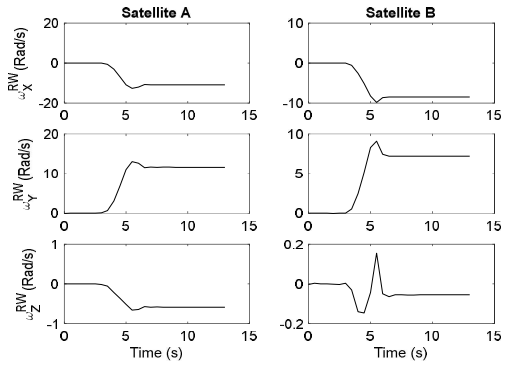

Fig. 18. The control torque applied by reaction wheels in deployment phase in case of failure of a tether.

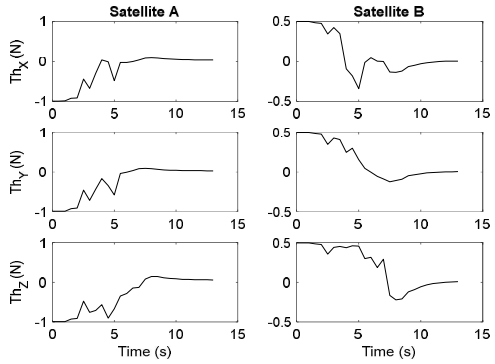

Fig. 19. The control effort applied by the thrusters in the deployment phase in case of failure of a tether.

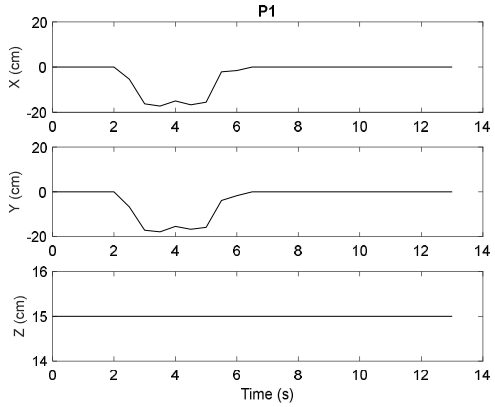

Fig. 20. The location of the junction points of the tether to the satellite B in the deployment phase in case of failure of a tether.

Monte-Carlo Simulation

The purpose of this section is to investigate the proposed control system's stability under various initial conditions. There are two general approaches to determining the stability of a control method. The first is a demonstration of analytical stability, while the second is a statistical analysis using Monte-Carlo simulation. Certain control methods have mathematical proofs of stability, which are referred to in this field as Lyapunov stability. To demonstrate the model predictive control method's stability, some works, such as [36], have suggested the use of the Lyapunov function in the cost function. Due to the difficulty or impossibility of determining the Lyapunov function in some systems, such as the one discussed in this paper, the second approach can be implemented using Monte-Carlo simulation. This is accomplished by simulating and controlling the introduced system in sufficient numbers (so that the average error does not change significantly as the number of runs increases) using a range of stochastic initial conditions specified in Table 5. The maximum values, mean, and standard deviation of the final errors for the state variables under model predictive control are shown in Table 6.

Table 5. Initial conditions for Monte-Carlo simulations.

Parameter	Initial Condition	Desired Condition
$\boldsymbol{L}$ (m)	$[3 \pm 2 \quad 4 \pm 2 \quad 5 \pm 2]$	$[3 \quad 4 \quad 5]^T$
$(\phi \quad \theta \quad \psi)_A$ (Deg)	$[\pm 90 \quad \pm 90 \quad \pm 90]$	$[0 \quad 0 \quad 0]^T$
$(\phi \quad \theta \quad \psi)_B$ (Deg)	$[\pm 90 \quad \pm 90 \quad \pm 90]$	$[0 \quad 0 \quad 0]^T$
$\boldsymbol{\omega}_A$ (Deg/s)	$[\pm 20 \quad \pm 20 \quad \pm 20]$	$[0 \quad 0 \quad 0]^T$
$\boldsymbol{\omega}_B$ (Deg/s)	$[\pm 20 \quad \pm 20 \quad \pm 20]$	$[0 \quad 0 \quad 0]^T$

Table 6. Mean and variance of control error in Monte-Carlo simulation.

Parameter	Position (m)	Velocity (m/s)	Angles (deg)	Angular Velocity (deg/s)
Average Error	0.05	0.003	0.09	0.01
Error Standard Deviation	0.015	0.001	0.025	0.002
Maximum Error	0.098	0.008	0.19	0.021

Additionally, Fig. 21 illustrates the behavior of the first satellite's angular velocity changes in Monte-Carlo simulations, demonstrating that the satellite's attitude is controlled and stable under a variety of different and non-zero initial conditions. In this regard, the tether deployment and retraction scenarios discussed in this chapter were chosen at random based on the initial conditions for each performance. As can be seen, the mean error is extremely low for both the position and attitude. Additionally, the maximum error of the controlled variables is very small, indicating the control system's stability. On the other hand, extremely low variance values for the final control error indicate that this control system is highly resistant to initial accidental conditions. Overall, the Monte-Carlo simulation results indicate that the proposed control method, regardless of the system's initial conditions, is capable of accurately controlling the system and preventing it from diverging.

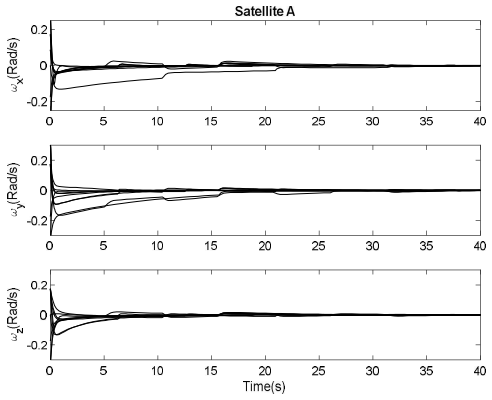

Fig. 21. The angular velocities of satellite A in Monte-Carlo simulation

Conclusion

The tether satellite system, which is connected via two tethers and moves in an elliptical orbit, was modeled in this paper using a three-dimensional Cartesian system. The proposed model took into account the coupling between the angles and movements of the tether and the attitude and position of the two satellites. The purpose of this paper is to present an fault-tolerant control method that utilizes a combination of tether traction control and the distance between the satellite's tethers' connection to the center of mass and the thruster. The method for fault-tolerant control is based on model predictive control (MPC). During the system's deployment phase prior to failure, the control model presented performed satisfactorily and was capable of generating the necessary controls. Due to the model's dependencies, the attitude perturbations are well controlled. After the failure of tether in deployment phase, the control implemented following the failure was able to dampen the disturbances caused by the rupture of a tether and by combining control methods. Despite the failure of the satellite system, the retraction phase was able to achieve the system's objective with minimal control effort by utilizing a combination of defined controls.

References

[1] P. K. Aravind, "The physics of the space elevator," American Journal of Physics, vol. 75, no. 2, 2007.
[2] S. Sasaki, K. Oyama and N. Kawashima, "Results from a series of tethered rocket experiments," Journal of Spacecraft and Rockets, vol. 24, no. 5, pp. 444-453, 1987.
[3] M. Cosmo and E. Lorenzini, "Tethers in Space Handbook," NASA, Washington DC, 1997.
[4] M. Kruijff, "The Young Engineers' satellite: flight results and critical analysis of a super-fast hands-on satellite project," in The 50th International Astronautical Congress, Greece, 1999.
[5] P. Williams, A. Hyslop, M. Stelzer and M. Kruijff, "YES2 optimal trajectories in presence of eccentricity and aerodynamic drag," Acta Astronautica, vol. 64, no. 7–8, pp. 745-769, 2009.
[6] S. Gates, S. Koss and M. Zedd, "Advanced Tether Experiment Deployment Failure," Journal of Spacecraft and Rockets, vol. 38, no. 1, pp. 60-68, 2001.
[7] R. Hoyt, J. Slostad and A. Mazzoleni, "The multiapplication survivable tether (MAST) experiment," in The 39th AIAA, ASME, SAE, ASEE Joint Propulsion Conference and Exhibit, Alabama, 2003.
[8] P. Velez, T. Atie, D. Alazard and C. Cumer, "Space Debris Removal using a Tether: A Model," IFACPapersOnLine, vol. 50, no. 1, pp. 7247-7252, 2017.
[9] A. K. Misra and G. S. Diamond, "Dynamics of a subsatellite system supported by two tethers," Journal of Guidance, Control, and Dynamics, vol. 9, no. 1, pp. 12- 16, 1986.
[10] K. Kumar and K. D. Kumar, "Line-of-Sight Pointing Stability for Drifting Satellites," IEEE Transactions on Aerospace and Electronic Systems, vol. 35, no. 2, pp. 504-510, 1999.
[11] V. J. Modi, "Spacecraft Attitude Dynamics: Evolution and Current Challenges," Acta Astronautica, vol. 21, no. 10, pp. 689-718, 1990.
[12] V. J. Modi, P. K. Lakshmanan and A. K. Misra, "Offset Control Strategy for the Space Station Based Tethered Payload," Astronautical Sciences, vol. 39, no. 2, pp. 205 232, 1991.
[13] A. Darabi and N. Assadian, "Coupled rotational and translational modeling of two satellites connected by a tether and their robust attitude control using optimal offset approach," Advances in Space Research, vol. 63, no. 8, pp. 2455-2468, 2019.
[14] P. Williams, T. Watanabe, B. C., P. Trivailo and H. A. Fuiji, "Libration Control of Flexible Tethers Using Electromagnetic Forces and Movable Attachment," Journal of Guidance, Control, and Dynamics, vol. 27, no. 5, pp. 882-897, 2004.
[15] Godard and K. D. Kumar, "Nonlinear optimal control of tethered satellite systems using tether offset in the presence of tether failure," Acta Astronautica, vol. 66, pp. 1434-1448, 2010.
[16] Godard, Kumar and B. Tan, "Fault tolerant stabilization of a tethered satellite system using offset control," Journal of Spacecraft and Rockets, vol. 45, no. 5, pp. 1070-1084, 2008.
[17] A. Misra, "Dynamics and control of tethered satellite systems," Acta Astronautica, vol. 63, pp. 1169-1177, 2008.
[18] G. Zhao, L. Sun and H. Huang, "Thrust control of tethered satellite with a short constant tether in orbital maneuvering," Aerospace Engineering, vol. 228, pp. 2569-2586, 2014.
[19] S. Yu, "Periodic motion in the tethered satellite system," Journal of Guidance, Control, and Dynamics, vol. 19, no. 5, pp. 1195-1197, 1996.
[20] K. Kumar, "Review on Dynamics and Control of Nonelectrodynamic Tethered Satellite Systems," Journal of Spacecraft and Rockets, vol. 43, no. 4, pp. 705-720, 2006.
[21] Z. Fan, H. Panfeng, M. Zhongjie and L. Zhengxiong, "Dynamics modeling and model selection of space debris

removal via the Tethered Space Robot," Proceedings of the Institution of Mechanical Engineers, Part G: Journal of Aerospace Engineering, vol. 231, no. 10, pp. 1873- 1897, 2016.
[22] T. Feng, M. Mingda and Z. Haihong, "Deployment control of long-distance space tether systems basd on parametric approach," in Proceedings of the 33rd Chinese Control Conference, Nanjing, 2014.
[23] J. Jin, S. Ko and C. Ryoo, "Fault tolerant control for satellites with four reaction wheels," Control Engineering practice, vol. 16, no. 10, pp. 1250-1258, 2008.
[24] E. F. Camacho and C. Bordons Alba, Model Predictive Control, London: Springer Verlag, 2007.
[25] M. Mirshams and M. Khosrojerdi, "Attitude control of an underactuated spacecraft using quaternion feedback regulator and tube-based MPC," Acta Astronautica, vol. 132, pp. 143-149, 2017.
[26] M. AllandiHallaj and N. Assadian, "Multiple-horizon multiple-model predictive control of electromagnetic tethered satellite system," Acta Astronautica, vol. 157, pp. 250-262, 2018.
[27] X. Wang, Z. Wang and Y. Zhang, "Model Predictive Control to Autonomously Approach a Failed Spacecraft," International Journal of Aerospace Engineering, vol. 2018, pp. 1-18, 2018.
[28] M. Tavakoli and N. Assadian, "Actuator failure-tolerant control of an all-thruster satellite in coupled translational and rotational motion using neural networks," International Journal of Adaptive Control and Signal Processing, vol. 32, no. 12, pp. 1748-1763, 2018.
[29] J. Scharnagl, P. Kremmydas and K. Schilling, "Model Predictive Control for Continuous Low Thrust Satellite Formation Flying," IFAC, vol. 51, no. 12, pp. 12-17, 2018.
[30] D. Vallado, Fundamentals of Astrodynamics and Applications, California: Microcosm Press, 2001.
[31] B. S. Yu, H. Wen and D. P. Jin, "Review of deployment technology for tethered satellite systems," Acta Mechanica Sinica, vol. 34, p. 754–768, 2018.
[32] R. Ramnath, Computation and Asymptotics, USA: Springer Briefs in Applied Sciencesand Technology, 2012.
[33] M. J. Sidi, Spacecraft Dynamics and Control, New York: Cambridge University Press, 1997.
[34] J. R. Wertz, Spacecraft Attitude Determination and Control, London: Springer Science & Business Media, 1978.
[35] M. Blanke, M. Staroswiecki and N. Wu, "Concepts and methods in fault-tolerant control," in Proceedings of the 2001 American Control Conference, Arlington, 2001.
[36] M. Diehl, R. Amrit and J. B. Rawlings, "A Lyapunov Function for Economic Optimizing Model Predictive Control," IEEE Transactions on Automatic Control, vol. 56, no. 3, pp. 703 - 707, 2011.